bioRxiv preprint doi: https://doi.org/10.1101/505131; this version posted December 23, 2018. The copyright holder for this preprint (which was not certified by peer review) is the author/funder. All rights reserved. No reuse allowed without permission.

Pleistocene Mammal Population Fluctuation Patterns Inferred by Their Genomes

Yulu Liu[1,#], Biao Liu[1,#], Xingxin Pan[1], Qiong Shi[1], Zhoujian Xiao[2], Shengbin Li[2,3,*], Shuaicheng Li[4,*]

[1]BGI Education Center, University of Chinese Academy of Sciences, Shenzhen 518083, China

[2]Forensics Genomics International (FGI), BGI-Shenzhen, Shenzhen 518083, China

[3]Shenzhen Key Laboratory of Forensics, BGI-Shenzhen, Shenzhen 518083, China

[4]Department of Computer Science, City University of Hong Kong, Hong Kong 999077, China

[#] these authors contributed equally to this study

[*]**Correspondence:** silkroad@genomics.cn, shuaicli@gmail.com

bioRxiv preprint doi: https://doi.org/10.1101/505131; this version posted December 23, 2018. The copyright holder for this preprint (which was not certified by peer review) is the author/funder. All rights reserved. No reuse allowed without permission.

Summary

Paleoclimate fluctuations critically affect paleoecological systems and influence mammal populations, even resulting in population differentiation [1]. Historical effective population size (N_e) can reflect these influences [2, 3]. Dozens of recent studies have investigated the relationship between variations in N_e values of one or a small number of mammalian species, inferred from genomic data, and fluctuations in paleoclimate [4-7]. However, there lacks an integrated and comprehensive study on the relationship between the fluctuations in paleoclimate and variations in N_e values inferred from genome sequencing data of a wide range of mammals. To investigate patterns in mammalian N_e values during the the Pleistocene, we gathered whole genome sequencing data of 60 mammals from 35 species distributed across Afro-Eurasia and the Americas, then inferred their N_e curves using the Pairwise Sequentially Markovian Coalescent (PSMC) method; 30 mammalian N_e curves almost simultaneously started to contract at the turning point of the Middle Pleistocene Transition (MPT); then the population of seven mammals started to expand at the turning point of the Middle Brunhes Event (MBE), while the contraction of other mammals' populations was prolonged to the later different time periods. Eight mammals experienced a severe population contraction around the Last Glaciation Maximum, as some aves did [8], while four potential ruminant beneficiaries showed an expanding population. *Sus scrofa* and *Bos taurus* experienced an internal population differentiation in the MPT. To conclude, the phenomenon that critical paleoclimate events

bioRxiv preprint doi: https://doi.org/10.1101/505131; this version posted December 23, 2018. The copyright holder for this preprint (which was not certified by peer review) is the author/funder. All rights reserved. No reuse allowed without permission.

35 facilitated contemporaneous animal population fluctuations in the paleoecological system

36 is showed by our N_e curve analysis.

37

38 **Keywords**: PSMC, mammal N_e, PCA, MPT

39

bioRxiv preprint doi: https://doi.org/10.1101/505131; this version posted December 23, 2018. The copyright holder for this preprint (which was not certified by peer review) is the author/funder. All rights reserved. No reuse allowed without permission.

RESULTS AND DISCUSSION

Effective population size of mammals during the Pleistocene

By utilizing the nonuniform distribution of single nucleotide variants (SNVs) in the genome, the Pairwise Sequentially Markovian Coalescent (PSMC) method can reconstruct the historical effective population size (N_e) from any single individual of the population [4]. In this work, we applied the PSMC method to obtain the N_e curves of 35 mammal species in Afro-Eurasia and the Americas (Figure S1). The N_e curves estimated from the genome data span the whole Pleistocene, yielding us that were sufficient to conduct the subsequent analysis.

Climates contributed to the mammal N_e curves

N_e fluctuation could result from a combined effect of genetics, climate, locations, or other factors [8]. To understand the degree that climate contributed to the N_e curves, we extracted the principal components (PCs) from 60 N_e curves by the principal component analysis (PCA). PC1 and PC2 contributed variance ratios of 0.508 and 0.273, respectively (Figure 1A). PC1 accounts for most of the variance; however, after hierarchical clustering, no signals could be detected to support that PC1 is correlated with genetic background (Figure S2). This finding could suggest that the complex paleoclimate impact on the mammals. We clustered these mammals hierarchically with

bioRxiv preprint doi: https://doi.org/10.1101/505131; this version posted December 23, 2018. The copyright holder for this preprint (which was not certified by peer review) is the author/funder. All rights reserved. No reuse allowed without permission.

PC2 (Figure 1B) and discovered that in many mammals (*Ursus*, *Ponginae*, *Homo*, *Canis*, some subgroups in *Rhinopithecus* and some herbivorous mammals), their genetically close subgroups were clustered in the same branch, with the exception of *Bos* and *Sus*. Eurasian and African *Bos* clusters as well as Asian and European *Sus* clusters are separated by a clear boundary, reflecting a long separation time of their populations that will be elaborated in the following section. Hence, PC2 could be interpreted as the integrated effect of the inherent genetic characteristics and geographical locations on the mammals. In general, close locations imply similar climate conditions; therefore, fluctuations of mammal N_e curves can reflect the climates of the mammal ancestors confronting to some extent.

N_e curve extrema clustered into seven clusters

N_e curve extrema are consistent with significant climate events in the Pleistocene. These extrema (Table S1) are centered at seven time points with an average silhouette coefficient of 0.64, --an acceptable cluster indicator. All seven clusters coincide with turning points of important climate events, as elaborated below.

The earliest cluster centered at 0.97±0.021 mya, with 40 extrema, coincided with the turning point of the Middle Pleistocene Transition (MPT, 0.94 mya [9]). We refer to this cluster as the MPT Cluster. In the MPT Cluster, 30 N_e curves reached a peak, including those of *Sus*, *Bos*, *Ovis*, *Capra*, *Equus caballus*, *Ailuropoda melanoleuca*, *Rhinopithecus*

bioRxiv preprint doi: https://doi.org/10.1101/505131; this version posted December 23, 2018. The copyright holder for this preprint (which was not certified by peer review) is the author/funder. All rights reserved. No reuse allowed without permission.

roxellana, *Rhinopithecus strykeri*, *Ursus arctos*, *Ursus maritimus*, *Pan troglodytes verus* and *Gorilla gorilla diehli*; and ten N_e curves displayed a bottleneck, including *Homo* and five species from *Equus*. Accordingly, we categorized the mammals into three classes (Table S1): MPT Maxima Class, MPT Minima Class, and MPT Neutral Class (mammals whose N_e curves are without the first extremum in the MPT class).

The contraction of the MPT Maxima Class around 0.97±0.021 mya may result from the Jaramillo geomagnetic reversal (1.07 mya~0.99 mya) [10] or changes in solar insolation after the coeval $\delta^{13}C_{max\text{-}III}$ event of 1.0~0.95 mya (Marine isotope stage (MIS) 29–25) [11, 12]. The climate became too harsh at a large scale for mammals to survive [9] and led to massive mammal extinction or population contraction events such as warm-steppic mammals being replaced with cold-steppic mammals in European Villafrancian fauna [13] and the southern-migration mammal wreck event of Gongwangling fauna [14]. The Plio-Pleistocene contributed substantially to current biomes [15] and MP fossils of 73.3% mammals in this class, including *Ailuropoda* [16], *Bos* [17], *Capra* [18], *Equus* [19], *Rhinopithecus* [20] and *Sus* [21] are majorly distributed in the Palearctic, according to the fossil database (Figure S3A, B, D, E, K and L). Therefore, the population peak of the MPT Maxima Class in the MPT Cluster suggests that the ancient populations of MP mammals in the Palearctic could have experienced severe contractions around the turning point of the MPT.

bioRxiv preprint doi: https://doi.org/10.1101/505131; this version posted December 23, 2018. The copyright holder for this preprint (which was not certified by peer review) is the author/funder. All rights reserved. No reuse allowed without permission.

The MPT Maxima Class population started to contract from the MPT Cluster center, and their first bottlenecks after that are distributed in five clusters (Figure 3A). The MPT Maxima Class, including African *Pan troglodytes verus* and *Bos*, wild-spread *Equus* and European *Sus Scrofa,* reached the first bottleneck at 0.43±0.018 mya, which is referred to as the MBE (Middle Brunhes Event) Bottleneck for 0.43 mya is happens to be the turning point of the MBE (MIS13-MIS11) [22]. Eight mammals, including *Capara*, Asian *Sus scrofa*, *Ovis aries*, and *Bos indicus*, reached the first bottleneck of their population at approximately 0.32±0.01 mya, the time which was known during the Mindel-Riss interglacial [23] (MRI bottleneck). These mammals, except the *Bos indicus*, were sampled at a relatively high latitude. In the Mindel-Riss interglacial, the climate was similar to the current climate. For four mammals including *Ursus arctos*, *Ursus maritimus* and two *Bos taurus* individuals, their ancestral N_e values synchronously reached the first bottleneck at 0.22±0.010 mya in the middle of the Riss glaciation, which is a relatively weak MIS 7 period with a cool interglaciation climate [24] (MRG Bottleneck). For nine mammals from the MPT Maxima Class, including *Ovis ammon polii*, *Ailuropoda melanoleuca*, *Bos grunniens*, *Rhinopithecus roxellana* and *Sus celebensis* as well as three *Bos taurus* individuals and one *Sus scrofa* individual, their ancestral N_e values started to show an expansion of their populations until 0.12±0.008 mya in the warmest, last interglaciation, the Eemian interglaciation [25] (EI Bottleneck). Two species, *Gorilla gorilla diehli* and *Rhinopithecus strykeri*, reached the first bottleneck until 0.04±0.004 mya (the most recent

bioRxiv preprint doi: https://doi.org/10.1101/505131; this version posted December 23, 2018. The copyright holder for this preprint (which was not certified by peer review) is the author/funder. All rights reserved. No reuse allowed without permission.

119 cluster center). These mammal populations contracted almost simultaneously but started
120 to expand at different time period.

121 Climate conditions could prompt mammal population migration and differentiation.
122 As a result, the population of migrated mammals may have started to expand, while
123 mammals that did not migrate sustained contraction. In the MPT Maxima Class, the
124 mammals that experienced the MBE Bottleneck likely lived in low latitude regions, and
125 those that experienced the MRI Bottleneck usually resided at relatively high latitudes with
126 the exception of *Bos* and *Sus scrofa*, which will be elaborated in the following section.
127 However, there was no obvious association between population fluctuations and habitats
128 of the mammals that experienced the MGR and EI bottlenecks. The fact that mammals in
129 the MPT Maxima Class spread in different latitudes, adapted themselves to different
130 environments and developed different habits, but shared five asynchronous expansion
131 times, could result from combined factors of environment in different latitudes and the
132 capacity for mammalian adaptations.

133 We also noticed that ten mammals of the MPT Neutral Class (Figure 3C) reached
134 a bottleneck while three of them reached a peak, at 0.67±0.030 mya, or the end of the
135 MPT. At that time, the planet held a high ice volume but was relatively warm [24, 27]. The
136 mammals that underwent a bottleneck around 0.67±0.030 mya included *Pongo*
137 *pygmaeus*, *Ursus americanus* *Macaca mulatta lasiota*, *Macaca thibetana* and *Canis*.
138 Their populations began to shrink separately before 1 mya, indicating that the population

bioRxiv preprint doi: https://doi.org/10.1101/505131; this version posted December 23, 2018. The copyright holder for this preprint (which was not certified by peer review) is the author/funder. All rights reserved. No reuse allowed without permission.

139 contraction impetus differed for mammals from the MPT Maxima Class. The mammals
140 with a peak at that time included *Odocoileus virginianus texanus*, *Gorilla gorilla gorilla* and
141 *Gorilla beringei graueri*.
142
143 ***Differentiation in mammal populations***
144 *Sus scrofa* and *Bos* populations experienced internal population differentiation between
145 0.97 mya and 0.43 mya in the middle Pleistocene transmission.
146 *Sus scrofa* belongs to the MPT Maxima Class (Table S1); thereafter, the
147 population of European *Sus scrofa* experienced a prolonged contraction until the MBE
148 Bottleneck, while the population of Asian *Sus scrofa* continued contracting until the MRG
149 Bottleneck (Figure 4A). The middle Pleistocene fossils of Asian *Sus scrofa* were only
150 distributed in relatively low latitude areas in Asia (Figure S3L). We also noticed that some
151 Asian mammals, such as *Capra aegagrus*, *Capra hircus* [18], and *Ailuropoda*
152 *melanoleuca* [16], also started their population expansion at the MRG Bottleneck, while
153 the European *Sus scrofa* population started to expand at the turning point of the MBE,
154 which is the same time as the *Equus caballus* population did [19]. The long-term
155 population contraction of Eurasian *Sus scrofa*, following a different fluctuation trend in the
156 MBE Bottleneck, indicates a differentiation in Eurasian *Sus scrofa* during the MPT and
157 MBE. Kijas estimated that Eurasian *Sus scrofa* maternity divergence time is ~0.9 mya
158 according to the mtDNA genome sequence [32]; with synonymous and nonsynonymous

bioRxiv preprint doi: https://doi.org/10.1101/505131; this version posted December 23, 2018. The copyright holder for this preprint (which was not certified by peer review) is the author/funder. All rights reserved. No reuse allowed without permission.

159 nucleotide substitutions of two main domains of the D-loop region in the cytochrome B
160 gene (CytB) (1,847 bp), Alves estimated the Eurasian *Sus scrofa* divergence time to be
161 ~0.6 mya [33]. Based on interpopulational distances for the mtDNA CytB sequence
162 (1,140 bp), another estimated divergence time is ~0.5 mya [33, 34]. With phylogenetic
163 analysis based on pairwise genetic distance of the mitotypes of Eurasian *Sus scrofa*,
164 using an evolutionary rate of 2%, their divergence time was estimated as 0.28 mya;
165 according to mtDNA D-loop sequence divergence time analysis, the Eurasian *Sus scrofa*
166 divergence time is ~58 kya [35]. Our N_e curves analysis support that Eurasian *Sus scrofa*
167 could have differentiated in 0.9~0.5 mya (during the long, harsh MPT [9]). The
168 estimations that the divergence time of Eurasian *Sus scrofa* is ~0.28 mya or ~58 kya
169 could have resulted from the inadequate sequence lengths used for the respective
170 estimations.

171 We noticed that for all the *Bos* individuals, their ancestral populations peaked at
172 the MPT Maxima Class as *Sus* did, while they experienced their subsequent bottlenecks
173 at different clusters (Figure 3A). The first population bottleneck of African *Bos indicus* and
174 one African *Bos taurus* located in the MBE bottleneck while Eurasian *Bos taurus* reached
175 the first bottleneck at later different cluster (Figure 4B), this phenomenon indicates that
176 the differentiation of the *Bos taurus* population occurred prior to the MBE bottleneck.
177 Since 92% mammals from MPT Maxima class are Palearctic mammals or Indomalayan
178 mammals exclude African *Bos*, the potential *Bos* population could originate in Palearctic.

bioRxiv preprint doi: https://doi.org/10.1101/505131; this version posted December 23, 2018. The copyright holder for this preprint (which was not certified by peer review) is the author/funder. All rights reserved. No reuse allowed without permission.

179 The first *Bos* fossil in Ethiopia originated in ~0.6 mya, indicating a migration of *Bos* [36].
180 which is also consistent with our estimated *Bos taurus* differentiation event, and because
181 of their potential ancestral population originated in the Palearctic, we could infer that their
182 migration direction is from Eurasia to Africa. Consequently, the harsh MPT period could
183 also result in the migration and differentiation of *Bos taurus*.
184
185 ***The fluctuation of mammal N_e in the Late Pleistocene (LP) period***
186 The N_e curves of many mammals fluctuated during the LP period. Around the time of the
187 LGM and Younger Dryas Event (YDE) (12.6~11.6 kya) [28, 29], the ancestral populations
188 of seven mammal species, including *Equus hemionus onager*, *Macaca nemestrina*,
189 *Equus quagga boehmi*, *Canis lupus*, *Odocoileus virginianus texanus*, and *Equus caballus*,
190 displayed a sudden contraction (Figure S4A). Furthermore, the populations of four
191 species, including *Capra aegagrus*, *Gorilla gorilla diehli* and non-African *Homo sapiens*,
192 experienced a sharp increase (Figure S4B).
193 The aforementioned fluctuation was accompanied by a megafauna extinction
194 during which many large mammals extricated [37-40]. The time of coincidence of the two
195 events indicates that the causes of the megafauna extinction event could also have
196 intensively influenced the ancestors who experienced the aforementioned decline event
197 of the extant mammals. The LGM and the YDE could have contributed to the ancient
198 mammal N_e decline event as well as the megafauna extinction event [37]. Many Aves

bioRxiv preprint doi: https://doi.org/10.1101/505131; this version posted December 23, 2018. The copyright holder for this preprint (which was not certified by peer review) is the author/funder. All rights reserved. No reuse allowed without permission.

199 populations also displayed such fluctuations at the same time, as indicated by their N_e
200 curves [8]. However, neither the LGM nor the YDE was solely sufficient to extinguish
201 megafauna [41], nor could they be the only substantial causes for the N_e decline event.
202 Hence, there could be other factors contributing to these two events.
203 *Homo sapiens* ancestors could also have contributed to the N_e fluctuations. In our
204 results, the N_e curves of *Canis lupus familiaris* and *Canis lupus* started their divergences
205 ~0.1 mya, corroborating that the estimated divergence time of the early dog and wolf
206 could be as early as 135 kya [42]. The N_e of the ancestor of *Canis lupus* experienced a
207 sudden, sharp decline event around the YDE, while the ancestor of *Canis lupus familiaris*
208 escaped such a decline (Figure 4C). According to recent research, *Canis lupus familiaris*
209 was domesticated in China in ~33 kya [43], in Central Asia in ~12.5 kya or in Europe in
210 ~15 kya [44]. The domestication events occurred around a population contraction event
211 of *Canis lupus,* the ancestor of which lived without domestication by *Homo sapiens*.
212 Therefore, humans could be related to the expansion of the *Canis lupus familiaris*
213 ancestral population. In the last glaciation, *Homo sapiens* started to spread across the
214 world from Africa with brilliant hunting ability in ~60 kya [45]. Encountering these clever
215 hunters, megafauna seldom understood how to survive. Many mammal N_e decline events
216 also happened after *Homo sapiens* spread, according to our results (Figure S4A). The
217 *Homo sapiens* spreading and occupancies agree with the time and trace for the extinction
218 of mammoths [37, 46, 47]. This hints that *Homo sapiens* could have played an essential

bioRxiv preprint doi: https://doi.org/10.1101/505131; this version posted December 23, 2018. The copyright holder for this preprint (which was not certified by peer review) is the author/funder. All rights reserved. No reuse allowed without permission.

role in modern mammal ancestral N_e contractions in the LP. Furthermore, the sharp expansion of *Bos indicus*-2, *Capra aegagrus* and *Gorilla gorilla diehli* after the LGM could also be attributed to mammalian ancestor population LP contractions and megafauna extinctions. Their population contraction event vacated ecological niches; thereafter, hostile environment adaptive ruminants such as *Bos* and *Capra* could have been the potential beneficiaries during this harsh period, and the domestication of *Homo sapiens* could also have facilitated their population expansion after the YDE [48].

DISCUSSION

Considering earth as a system, paleoclimate fluctuations affect the rise and fall of the population of earth's creatures in the paleoecological system. N_e curves inferred by PSMC analysis offer a chance to investigate N_e dynamics in ancient times, and fossil distributions can verify these results. The influences of the MPT, MBE, LGM and other paleoclimate events on the paleoecosystem are obviously reflected in the mammal N_e curves. Furthermore, the analysis of these mammal N_e curves reveals preliminary impacts of climate fluctuations on the biosphere. In addition, the mammal N_e decline events in harsh stages alert us to pay attention to the dangers that could be caused by dramatic climate change in the future.

ACKNOWLEDGMENTS

bioRxiv preprint doi: https://doi.org/10.1101/505131; this version posted December 23, 2018. The copyright holder for this preprint (which was not certified by peer review) is the author/funder. All rights reserved. No reuse allowed without permission.

We are grateful to Yanlin zhang (McGill) for excellent technical help.; andwe thank Bailiang Jian (BGI) and Yilin Liu (BGI) for improving the manuscript;we also acknowledge BGI-Shenzhen for the computing resources;

we thank Fossilworks and the contributors who provided fossil records for us, including the following:

A. Behrensmeyer. Taxonomic occurrences of mammal recorded in the fossilworks. http://fossilworks.org.

A. Hendy. Taxonomic occurrences of mammal recorded in the PaleoDB. http://fossilworks.org.

A. Miller. Taxonomic occurrences of Equus recorded in the PaleoDB. http://fossilworks.org.

A. Turner. Taxonomic occurrences of mammal recorded in the PaleoDB. http://fossilworks.org.

C. Bell. Taxonomic occurrences of mammal recorded in the PaleoDB. http://fossilworks.org.

C. Jaramillo. Taxonomic occurrences of mammal recorded in the PaleoDB. http://fossilworks.org.

D. Croft. Taxonomic occurrences of mammal recorded in the PaleoDB. http://fossilworks.org.

E. Fara. Taxonomic occurrences of B recorded in the PaleoDB. http://fossilworks.org.

bioRxiv preprint doi: https://doi.org/10.1101/505131; this version posted December 23, 2018. The copyright holder for this preprint (which was not certified by peer review) is the author/funder. All rights reserved. No reuse allowed without permission.

E. Vlachos. Taxonomic occurrences of Bos recorded . http://fossilworks.org.

J. Alroy. Taxonomic occurrences of mammal recorded in the Fossilworks.

http://fossilworks.org.

J. Bloch. Taxonomic occurrences of mammal recorded. http://fossilworks.org.

J. Marcot. Taxonomic occurrences of mammal recorded. http://fossilworks.org.

M. Carrano. Taxonomic occurrences of mammal recorded in the PaleoDB.

http://fossilworks.org.

M. Uhen. Taxonomic occurrences of mammal recorded in the PaleoDB.

http://fossilworks.org.

P. Holroyd. Taxonomic occurrences of Equus recorded. http://fossilworks.org.

P. Mannion. Taxonomic occurrences of Equus recorded in the PaleoDB.

http://fossilworks.org.

W. Clyde. Taxonomic occurrences of mammal recorded in the PaleoDB.

http://fossilworks.org.

W. Kiessling. Taxonomic occurrences of Macaca recorded. http://fossilworks.org.

AUTHOR CONTRIBUTIONS

S.C.L. supervised the research and revised the manuscript; Y.L.L. collected, analyzed data and prepared the manuscript draft; B.L. participated in the literature review and

bioRxiv preprint doi: https://doi.org/10.1101/505131; this version posted December 23, 2018. The copyright holder for this preprint (which was not certified by peer review) is the author/funder. All rights reserved. No reuse allowed without permission.

278 performed some analysis; X.X.P. collected some datasets; Z.J.X provided assistance;

279 Q.S supervised the research; S.B.L revised the manuscripts.

280

281 **DECLARATION OF INTERESTS**

282 The authors declare no competing interests.

283

bioRxiv preprint doi: https://doi.org/10.1101/505131; this version posted December 23, 2018. The copyright holder for this preprint (which was not certified by peer review) is the author/funder. All rights reserved. No reuse allowed without permission.

REFERENCES

1. Williams, M.A., Dunkerley, D., De Deckker, P., Kershaw, A.P., and Stokes, T. (1993). Quaternary environments, (E. Arnold).
2. Wright, S. (1938). Size of population and breeding structure in relation to evolution. Science (New York, N.Y.) *87*, 430-431.
3. Hofreiter, M., and Stewart, J. (2009). Ecological change, range fluctuations and population dynamics during the Pleistocene. Curr. Biol. *19*, R584–R594.
4. Li, H., and Durbin, R. (2011). Inference of human population history from individual whole-genome sequences. Nature *475*, 493-496.
5. Zhao, S., Zheng, P., Dong, S., Zhan, X., Wu, Q., Guo, X., Hu, Y., He, W., Zhang, S., and Fan, W. (2013). Whole-genome sequencing of giant pandas provides insights into demographic history and local adaptation. Nature Genet. *45*, 67.
6. Higashino, A., Sakate, R., Kameoka, Y., Takahashi, I., Hirata, M., Tanuma, R., Masui, T., Yasutomi, Y., and Osada, N. (2012). Whole-genome sequencing and analysis of the Malaysian cynomolgus macaque (*Macaca fascicularis*) genome. Genome Biol. *13*, R58.
7. Miller, W., Schuster, S.C., Welch, A.J., Ratan, A., Bedoya-Reina, O.C., Zhao, F., Kim, H.L., Burhans, R.C., Drautz, D.I., Wittekindt, N.E., et al. (2012). Polar and brown bear genomes reveal ancient admixture and demographic footprints of past climate change. Proc. Natl. Acad. Sci. U. S. A. *109*, E2382–2390.
8. Nadachowska-Brzyska, K., Li, C., Smeds, L., Zhang, G., and Ellegren, H. (2015). Temporal dynamics of avian populations during Pleistocene revealed by whole-genome sequences. Curr. Biol. *25*, 1375–1380.
9. Head, M.J., and Gibbard, P.L. (2005). Early-middle Pleistocene transitions: an overview and recommendation for the defining boundary. Geol. Soc. Spec. Publ. *247*, 1–18.
10. Cande, S.C., and Kent, D.V. (1995). Revised calibration of the geomagnetic polarity timescale for the Late Cretaceous and Cenozoic. J. Geophys. Res. Solid Earth *100*, 6093–6095.
11. Wang, P., Li, Q., Tian, J., Jian, Z., Liu, C., Li, L., and Ma, W. (2014). Long-term cycles in the carbon reservoir of the Quaternary ocean: a perspective from the south China sea. Nat. Sci. Rev. *1*, 119–143.
12. Pälike, H., Norris, R.D., Herrle, J.O., Wilson, P.A., Coxall, H.K., Lear, C.H., Shackleton, N.J., Tripati, A.K., and Wade, B.S. (2006). The heartbeat of the Oligocene climate system. Science (New York, N.Y.) *314*, 1894-1898.
13. Rook, L., and Martínez-Navarro, B. (2010). Villafranchian: the long story of a Plio-Pleistocene European large mammal biochronologic unit. Quat. Int. *219*, 134–144.
14. Tong, H. (2007). Occurrences of warm-adapted mammals in north China over the Quaternary period and their paleo-environmental significance. Sci. China Ser. D Earth Sci. *50*, 1327–1340.
15. Pennington, R.T., Cronk, Q.C., and Richardson, J.A. (2004). Introduction and synthesis: plant phylogeny and the origin of major biomes. Philos. Trans. R. Soc. Lond. B Biol. Sci. *359*, 1455–

bioRxiv preprint doi: https://doi.org/10.1101/505131; this version posted December 23, 2018. The copyright holder for this preprint (which was not certified by peer review) is the author/funder. All rights reserved. No reuse allowed without permission.

1464.

16. Tsiang-Ke, W. (1974). On the taxonomic status of species, geological distribution and evolutionary history of Ailuropoda. Acta Zool. Sin. *2*, 010.

17. Van Vuure, C. (2005). Retracing the aurochs: history, morphology and ecology of an extinct wild ox, (Pensoft Pub).

18. Agusti, J., Oms, O., and Pares, J.M. (1999). Calibration of the Early-middle Pleistocene transition in the continental beds of the Guadix–Baza Basin (SE Spain). Quat. Sci. Rev. *18*, 1409–1417.

19. Eisenmann, V. (1992). Origins, dispersals, and migrations of Equus. (*Mammalia, Perissodactyla*). CFS Cour. Forschungsinstitut Senckenberg *153*, 161–170.

20. Takai, M., Zhang, Y., Kono, R.T., and Jin, C. (2014). Changes in the composition of the Pleistocene primate fauna in southern China. Quaternary International *354*, 75-85.

21. Rothschild, M.F., and Ruvinsky, A. (2011). The genetics of the pig, (CABI).

22. Wang, P., Tian, J., Cheng, X., Liu, C., and Xu, J. (2003). Carbon reservoir changes preceded major ice-sheet expansion at the mid-Brunhes event. Geology *31*, 239-242.

23. Fan, J., and Hou, X. (2018). International Chronostratigraphic Chart. Volume 2018.

24. Lang, N., and Wolff, E.W. (2011). Interglacial and glacial variability from the last 800 ka in marine, ice and terrestrial archives. Clim. Past *7*, 361–380.

25. Kolfschoten, T.v. (1992). Aspects of the migration of mammals to Northwestern Europe during the Pleistocene, in particular the reimmigration of Arvicola terrestris. Courier *153*, 213.

26. Hemming, S.R. (2004). Heinrich events: massive late pleistocene detritus layers of the North Atlantic and their global climate imprint. Rev. Geophy. *42*, doi: 10.1029/2003RG000128.

27. Clark, P.U., Archer, D., Pollard, D., Blum, J.D., Rial, J.A., Brovkin, V., Mix, A.C., Pisias, N.G., and Roy, M. (2006). The middle Pleistocene transition: characteristics, mechanisms, and implications for long-term changes in atmospheric pCO2. Quat. Sci. Rev. *25*, 3150–3184.

28. Clark, P.U., Dyke, A.S., Shakun, J.D., Carlson, A.E., Clark, J., Wohlfarth, B., Mitrovica, J.X., Hostetler, S.W., and McCabe, A.M. (2009). The Last Glacial Maximum. Science (New York, N.Y.) *325*, 710.

29. Firestone, R.B., West, A., Kennett, J.P., Becker, L., Bunch, T.E., Revay, Z.S., Schultz, P.H., Belgya, T., Kennett, D.J., Erlandson, J.M., et al. (2007). Evidence for an extraterrestrial impact 12,900 years ago that contributed to the megafaunal extinctions and the Younger Dryas cooling. Proc. Natl. Acad. Sci. U S A *104*, 16016–16021.

30. Mithen, S., and Straus, L. (2004). Archaeology-After the ice a global human history, 20,000-5000, (Cambridge, Mass: Science).

31. López-García, J., Blain, H.-A., Bennasar, M., Sanz, M., and Daura, J. (2013). Heinrich event 4 characterized by terrestrial proxies in southwestern Europe. Clim. Past *9*, 1053–1064.

32. Kijas, J., and Andersson, L. (2001). A phylogenetic study of the origin of the domestic pig estimated from the near-complete mtDNA genome. J. Mol. Evol. *52*, 302–308.

33. Alves, E., Ovilo, C., Rodriguez, M., and Silio, L. (2003). Mitochondrial DNA sequence variation and phylogenetic relationships among Iberian pigs and other domestic and wild pig populations. Anim.

bioRxiv preprint doi: https://doi.org/10.1101/505131; this version posted December 23, 2018. The copyright holder for this preprint (which was not certified by peer review) is the author/funder. All rights reserved. No reuse allowed without permission.

Genet. *34*, 319–324.

34. Giuffra, E., Kijas, J., Amarger, V., Carlborg, Ö., Jeon, J.-T., and Andersson, L. (2000). The origin of the domestic pig: independent domestication and subsequent introgression. Genetics *154*, 1785–1791.

35. Kim, K.I., Lee, J.H., Li, K., Zhang, Y.P., Lee, S.S., Gongora, J., and Moran, C. (2002). Phylogenetic relationships of Asian and European pig breeds determined by mitochondrial DNA D-loop sequence polymorphism. Anim. Genet. *33*, 19–25.

36. O'Regan, H.J., Turner, A., Bishop, L.C., Elton, S., and Lamb, A.L. (2011). Hominins without fellow travellers? First appearances and inferred dispersals of Afro-Eurasian large-mammals in the Plio-Pleistocene. Quaternary Science Reviews *30*, 1343-1352.

37. Gillespie, R. (2008). Updating Martin's global extinction model. Quat. Sci. Rev. *27*, 2522–2529.

38. Wroe, S., and Field, J. (2006). A review of the evidence for a human role in the extinction of Australian megafauna and an alternative interpretation. Quat. Sci. Rev. *25*, 2692–2703.

39. Alroy, J. (2001). A Multispecies Overkill Simulation of the End-Pleistocene Megafaunal Mass Extinction. Science (New York, N.Y.) *292*, 1893.

40. Koch, P.L., and Barnosky, A.D. (2006). Late quaternary extinctions: state of the debate. Annu. Rev. Ecol. Evol. Syst. *37*, 215–250.

41. Martin, P.S. (1984). Prehistoric overkill: the global model. In Quaternary extinctions: a prehistoric revolution, P.S. Martin and G.K. Richard, eds. (USA: The University of Arizona Press), pp. 354–403.

42. Freedman, A.H., and Wayne, R.K. (2017). Deciphering the origin of dogs: from fossils to genomes. Annu. Rev. Anim. Biosci. *5*, 281–307.

43. Wang, G.-D., Zhai, W., Yang, H.-C., Wang, L., Zhong, L., Liu, Y.-H., Fan, R.-X., Yin, T.-T., Zhu, C.-L., and Poyarkov, A.D. (2016). Out of southern East Asia: the natural history of domestic dogs across the world. Cell Res. *26*, 21.

44. Frantz, L.A., Mullin, V.E., Pionnier-Capitan, M., Lebrasseur, O., Ollivier, M., Perri, A., Linderholm, A., Mattiangeli, V., Teasdale, M.D., and Dimopoulos, E.A. (2016). Genomic and archaeological evidence suggest a dual origin of domestic dogs. Science (New York, N.Y.) *352*, 1228-1231.

45. Callaway, E. (2018). Israeli fossils are the oldest modern humans ever found outside of Africa. Nature *554*, 15-16.

46. Stuart, A.J. (2005). The extinction of woolly mammoth (Mammuthus primigenius) and straight-tusked elephant (*Palaeoloxodon antiquus*) in Europe. Quat. Int. *126-128*, 171–177.

47. Martin, P.S., and Stuart, A.J. (2016). Mammoth Extinction: Two Continents and Wrangel Island. Radiocarbon *37*, 7-10.

48. Vigne, J.-D. (2011). The origins of animal domestication and husbandry: a major change in the history of humanity and the biosphere. C. R. Biol. *334*, 171–181.

49. Kim, J., Hanotte, O., Mwai, O.A., Dessie, T., Bashir, S., Diallo, B., Agaba, M., Kim, K., Kwak, W., Sung, S., et al. (2017). The genome landscape of indigenous African cattle. Genome Biol. *18*, 34.

bioRxiv preprint doi: https://doi.org/10.1101/505131; this version posted December 23, 2018. The copyright holder for this preprint (which was not certified by peer review) is the author/funder. All rights reserved. No reuse allowed without permission.

50. Lee, H.J., Kim, J., Lee, T., Son, J.K., Yoon, H.B., Baek, K.S., Jeong, J.Y., Cho, Y.M., Lee, K.T., Yang, B.C., et al. (2014). Deciphering the genetic blueprint behind Holstein milk proteins and production. Genome Biol. Evol. *6*, 1366–1374.

51. Kim, S.J., Ka, S., Ha, J.W., Kim, J., Yoo, D., Kim, K., Lee, H.K., Lim, D., Cho, S., Hanotte, O., et al. (2017). Cattle genome-wide analysis reveals genetic signatures in trypanotolerant N'Dama. BMC genomics *18*, 371.

52. Chen, Y., Chen, Y., Shi, C., Huang, Z., Zhang, Y., Li, S., Li, Y., Ye, J., Yu, C., Li, Z., et al. (2017). SOAPnuke: a mapreduce acceleration supported software for integrated quality control and preprocessing of high-throughput sequencing data. GigaScience *7*, 1–6.

53. Li, H., and Durbin, R. (2009). Fast and accurate short read alignment with Burrows–Wheeler transform. Bioinformatics *25*, 1754-1760.

bioRxiv preprint doi: https://doi.org/10.1101/505131; this version posted December 23, 2018. The copyright holder for this preprint (which was not certified by peer review) is the author/funder. All rights reserved. No reuse allowed without permission.

411 **FIGURE LEGENDS**

412 **Figure 1. PC analysis of mammal demographic trajectories.** (A) PC1 and PC2 plots.
413 Different colors or shapes represent different mammal classes. (B) Clusters obtained
414 using PC2 of N_e curves. Colors represent mammal classes. *Bos* and *Sus* are marked by
415 triangles and pentagrams, respectively. Mammals in light gray shading share a close
416 genetic relationship and cluster closely when using PC2 of N_e curves. Mammals in dark
417 gray shadows share a relatively close genetic relationship, live in similar habitats, and
418 cluster closely when using PC2 of N_e curves. The scale bar represents the Euclidean
419 distance between samples.

420 **Figure 2**. **Sankey diagram of mammal extrema.** Mammals in the same column possess
421 the same extremum. Sample names are in Table S1.

422 **Figure 3. Sankey diagram of three classes.** (A) MPT Maxima Class. (B) MPT Minima
423 Class. (C) MPT Neutral Class. Sample names are also in Table S1.

424 **Figure 4. three mammal N_e curves.** (A)N_e curves of *Sus scrofa* and *Sus celebensis*;
425 (B)N_e curves of *Bos taurus*, *Bos indicus* and *Bos grunniens*; (C) N_e curves of *Canis lupus*
426 *familiaris* and *Canis lupus*-1.

427

bioRxiv preprint doi: https://doi.org/10.1101/505131; this version posted December 23, 2018. The copyright holder for this preprint (which was not certified by peer review) is the author/funder. All rights reserved. No reuse allowed without permission.

428

429 **STAR★METHODS**

430

431 **KEY RESOURCE TABLE**

REAGENT or RESOURCES	SOURCE	IDENTIFIER
Bos indicus-1	[49]	SRR3225526
Bos indicus-2	[49]	SRR3546787
Bos indicus-3	[49]	SRR3694652
Bos taurus-1	[49]	SRR3656921
Bos taurus-2	[49]	SRR3694478
Bos taurus-3	[50]	SRR934409
Bos taurus-4	[50]	SRR934402
Bos taurus-5	[51]	SRR3497611
Bos taurus-6	[51]	SRR3499149
Bos grunniens-1	[51]	SRR361224, SRR361227
Capra aegagrus-1	[52]	SRR1576690
Capra hircus-1	[53]	SRR488786, SRR488791, SRR488812, SRR488787, SRR488805, SRR488813
Ovis aries-1	[54]	SRR1217914, SRR1217915, SRR1217916, SRR1217917, SRR1217939, SRR1217905, SRR1217906, SRR1217907, SRR1217908, SRR1217909, SRR1217937, SRR1217910, SRR1217911, SRR1217912, SRR1217913, SRR1217938, SRR1217918, SRR1217919, SRR1217920, SRR1217921, SRR1217940
Ovis ammon polii-1	[55]	SRR5753922
Equus caballus-1	[56]	SRR1055837
Equus caballus-2	[56]	SRR1046151
Equus asinus-1	[56]	SRR873443, SRR873444, SRR873445
Equus quagga boehmi-1	[57]	ERR660704, ERR660705, ERR660706, ERR660707, ERR660708, ERR660709, ERR660710, ERR660711, ERR660712, ERR660713, ERR660714, ERR660715, ERR660717, ERR660716, ERR660718, ERR660719, ERR660720, ERR660721, ERR660722, ERR660723, ERR660724, ERR660725, ERR660726, ERR660727, ERR660728, ERR660729, ERR660730, ERR660731, ERR660732, ERR660733, ERR660734, ERR660735, ERR660736, ERR660737, ERR660738, ERR660739, ERR660740, ERR660741, ERR660742, ERR660743, ERR660744, ERR660745, ERR660746, ERR660747, ERR660748, ERR660749, ERR660750, ERR660751, ERR660752, ERR660753, ERR660754, ERR660755, ERR660756, ERR660757, ERR660758, ERR660759, ERR660760, ERR660761, ERR660762, ERR660763,

bioRxiv preprint doi: https://doi.org/10.1101/505131; this version posted December 23, 2018. The copyright holder for this preprint (which was not certified by peer review) is the author/funder. All rights reserved. No reuse allowed without permission.

		ERR660764, ERR660765, ERR660766, ERR660767, ERR660768, ERR660769, ERR660770, ERR660771, ERR660793, ERR660772, ERR660773, ERR660774, ERR660775, ERR660776, ERR660777, ERR660778, ERR660779, ERR660780, ERR660781, ERR660782, ERR660783, ERR660784, ERR660785, ERR660786, ERR660787, ERR660788, ERR660789, ERR660790, ERR660791, ERR660792, ERR660794, ERR660795, ERR660796, ERR660797, ERR660798, ERR660799, ERR660800, ERR660801, ERR660802, ERR660803, ERR660804, ERR660805, ERR660806, ERR660807, ERR660808, ERR660809, ERR660810, ERR660811, ERR660812, ERR660813, ERR660814, ERR660815, ERR660816, ERR660817, ERR660818, ERR660819, ERR660820
Equus grevyi-1	[57]	ERR669470, ERR669471, ERR669472, ERR669473, ERR669474, ERR669475, ERR669476, ERR669477, ERR669478, ERR669479, ERR669480, ERR669481, ERR669482, ERR669483, ERR669484, ERR669485, ERR669486, ERR669487, ERR669488, ERR669489, ERR669490, ERR669491, ERR669492, ERR669493, ERR669494, ERR669495, ERR669496, ERR669497, ERR669498, ERR669499, ERR669500, ERR669501, ERR669502, ERR669503, ERR669504, ERR669505, ERR669506, ERR669507, ERR669508, ERR669509, ERR669510, ERR669511, ERR669512, ERR669513, ERR669514, ERR669515, ERR669516, ERR669517, ERR669518, ERR669519, ERR669520, ERR669521, ERR669522, ERR669523, ERR669524, ERR669525, ERR669526, ERR669527, ERR669528, ERR669529, ERR669530, ERR669531, ERR669532, ERR669533, ERR669534, ERR669535, ERR669536, ERR669537, ERR669538, ERR669539, ERR669540, ERR669541, ERR669542, ERR669543, ERR669544, ERR669545, ERR669546, ERR669547, ERR669548, ERR669549, ERR669550, ERR669551, ERR669552, ERR669553, ERR669554, ERR669555, ERR669556, ERR669557, ERR669558, ERR669559, ERR669560, ERR669561, ERR669562, ERR669563
Equus zebra hartmannae-1	[57]	ERR657893, ERR657894, ERR657895, ERR657896, ERR657897, ERR657898, ERR657899, ERR657900, ERR657901, ERR657902, ERR657903, ERR657904, ERR657905, ERR657906, ERR657907, ERR657908, ERR657909, ERR657910, ERR657911, ERR657912, ERR657913, ERR657914, ERR657915, ERR657916, ERR657917, ERR657918, ERR657919, ERR657920, ERR657921, ERR657922, ERR657923, ERR657924, ERR657925, ERR657926, ERR657927, ERR657928, ERR657929, ERR657930, ERR657931, ERR657932, ERR657933, ERR657934, ERR657935, ERR657936, ERR657937, ERR657938, ERR657939, ERR657940, ERR657941, ERR657942, ERR657943, ERR657944, ERR657945, ERR657946, ERR657947, ERR657948,

bioRxiv preprint doi: https://doi.org/10.1101/505131; this version posted December 23, 2018. The copyright holder for this preprint (which was not certified by peer review) is the author/funder. All rights reserved. No reuse allowed without permission.

		ERR657949, ERR657950, ERR657951, ERR657952, ERR657953, ERR657954, ERR657955, ERR657956, ERR657957, ERR657958, ERR657959, ERR657960, ERR657961, ERR657962, ERR657963, ERR657964, ERR657965, ERR657966, ERR657967, ERR657968, ERR657969, ERR657970, ERR657971, ERR657972, ERR657973, ERR657974, ERR657975, ERR657976, ERR657977, ERR657978, ERR657979, ERR657980, ERR657981, ERR657982, ERR657983, ERR657984
Equus kiang-1	[57]	ERR669419, ERR669420, ERR669421, ERR669422, ERR669423, ERR669424, ERR669425, ERR669426, ERR669427, ERR669428, ERR669429, ERR669430, ERR669431, ERR669432, ERR669433, ERR669434, ERR669435, ERR669436, ERR669437, ERR669438, ERR669439, ERR669440, ERR669441, ERR669442, ERR669443, ERR669444, ERR669445, ERR669446, ERR669447, ERR669448, ERR669449, ERR669450, ERR669451, ERR669452, ERR669453, ERR669454, ERR669455, ERR669456, ERR669457, ERR669458, ERR669459, ERR669460, ERR669461, ERR669462, ERR669463, ERR669464, ERR669465, ERR669466, ERR669467, ERR669468, ERR669469
Equus hemionus onager-1	[57]	ERR654542, ERR654543, ERR654544, ERR654545, ERR654546, ERR654547, ERR654548, ERR654549, ERR654550, ERR654551, ERR654552, ERR654553, ERR654554, ERR654555, ERR654556, ERR654557, ERR654558, ERR654559, ERR654560, ERR654561, ERR654562, ERR654563, ERR654564, ERR654565, ERR654566, ERR654567, ERR654568, ERR654569, ERR654570, ERR654571, ERR654572, ERR654573, ERR654574, ERR654575, ERR654576, ERR654577, ERR654578, ERR654579, ERR654580, ERR654581, ERR654582, ERR654583, ERR654584, ERR654585, ERR654586, ERR654587, ERR654588, ERR654589, ERR654590, ERR654591, ERR654592, ERR654593, ERR654594, ERR654595, ERR654596, ERR654597, ERR654598, ERR654599, ERR654600, ERR654601, ERR654602, ERR654603, ERR654604, ERR654605, ERR654606, ERR654607, ERR654608, ERR654609, ERR654610, ERR654611, ERR654612
Equus africanus somaliensis-1	[57]	ERR650570, ERR650571, ERR650572, ERR650573, ERR650574, ERR650575, ERR650576, ERR650577, ERR650578, ERR650579, ERR650580, ERR650581, ERR650582, ERR650583, ERR650584, ERR650585, ERR650586, ERR650587, ERR650588, ERR650589, ERR650590, ERR650591, ERR650592, ERR650593, ERR650594, ERR650595, ERR650596, ERR650597, ERR650598, ERR650599, ERR650600, ERR650601, ERR650602, ERR650603, ERR650604, ERR650605, ERR650606, ERR650607, ERR650608, ERR650609, ERR650610, ERR650611, ERR650612, ERR650613, ERR650614, ERR650615, ERR650616, ERR650617, ERR650618, ERR650619, ERR650620, ERR650621,

bioRxiv preprint doi: https://doi.org/10.1101/505131; this version posted December 23, 2018. The copyright holder for this preprint (which was not certified by peer review) is the author/funder. All rights reserved. No reuse allowed without permission.

		ERR650622, ERR650623, ERR650624, ERR650625, ERR650626, ERR650627, ERR650628, ERR650629, ERR650630, ERR650631, ERR650632, ERR650633, ERR650634, ERR650635, ERR650636, ERR650637, ERR650638, ERR650639, ERR650640, ERR650641, ERR650642, ERR650643, ERR650644, ERR650645, ERR650646, ERR650647, ERR650648, ERR650649, ERR650650, ERR650651, ERR650652, ERR650653, ERR650654, ERR650655, ERR650656, ERR650657, ERR650658, ERR650659, ERR650660, ERR650661, ERR650662, ERR650663, ERR650664, ERR650665, ERR650666, ERR650667, ERR650668, ERR650669, ERR650670, ERR650671, ERR650672, ERR650673, ERR650674, ERR650675, ERR650676, ERR650677, ERR650678, ERR650679, ERR650680, ERR650681, ERR650682, ERR650683, ERR650684, ERR650685, ERR650686, ERR650687, ERR650688, ERR650689, ERR650690, ERR650691, ERR650692, ERR650693, ERR650694, ERR650695, ERR650696, ERR650697, ERR650698, ERR650699, ERR650700, ERR650701, ERR650702, ERR650703
Odocoileus virginianus texanus-1	[58]	SRR4069803, SRR4069806, SRR4069810, SRR4069815
Canis lupus familiaris-1	[59]	SRR2827578
Canis lupus familiaris-2	[59]	SRR2827588
Canis lupus familiaris-3	[59]	SRR2827594
Canis lupus familiaris-4	[59]	SRR2827563
Canis lupus familiaris-5	[60]	SRR1138369
Canis lupus-1	[59]	SRR2827600
Macaca mulatta lasiota-1	[61]	SRR278719, SRR278720, SRR278721, SRR278722, SRR278723, SRR278724, SRR278725, SRR278726, SRR278727, SRR278728, SRR278729, SRR278730, SRR278731, SRR278732, SRR278733, SRR278734, SRR278735, SRR278736, SRR278737, SRR278738, SRR278739, SRR278740
Macaca nemestrina-1		SRR1698391, SRR1698394
Macaca thibetana-1	[62]	SRR1024051
Rhinopithecus roxellana-1	[63]	SRR2017664
Rhinopithecus avunculus-1	[63]	SRR1588565
Rhinopithecus strykeri-1	[63]	SRR1588563
Rhinopithecus brelichi-1	[63]	SRR1588562
Sus scrofa-1	[64]	ERR173181
Sus scrofa-2	[64]	ERR173202

bioRxiv preprint doi: https://doi.org/10.1101/505131; this version posted December 23, 2018. The copyright holder for this preprint (which was not certified by peer review) is the author/funder. All rights reserved. No reuse allowed without permission.

Sus scrofa-3	[64]	ERR173217
Sus scrofa-4	[64]	ERR173222
Sus scrofa-5	[64]	ERR173176
Sus scrofa-6	[64]	SRR652446, SRR652448, SRR652449, SRR652450
Sus celebensis-1	[64]	ERR173210
Pongo pygmaeus-1	[65]	SRR748012, SRR748013, SRR748014
Pan troglodytes verus-1	[65]	SRR748081, SRR748082, SRR748083, SRR748084
Pan troglodytes schweinfurthii-1	[65]	SRR726412, SRR726413, SRR726415, SRR726416
Pan paniscus-1	[65]	SRR740831, SRR740832, SRR740835
Gorilla gorilla gorilla-1	[65]	SRR748177, SRR748178
Gorilla gorilla diehli-1	[65]	SRR748109, SRR748110, SRR748111, SRR748112
Gorilla beringei graueri-1	[65]	SRR747961, SRR747962
Homo sapiens-1	[66]	1000genomes
Homo sapiens-2	[66]	1000genomes
Homo sapiens-3	[66]	1000genomes
Homo sapiens-4	[67]	ERZ324532
Homo sapiens-5	[67]	ERZ324535
Ailuropoda melanoleuca-1	[68]	SRR2716726, SRR2717569, SRR2717570, SRR2717571
Ursus maritimus-1	[7]	SRR518683
Ursus arctos-1	[7]	SRR518712, SRR518713
Ursus americanus-1	[7]	SRR518723
Ailuropoda	http://fossilworks.org	13293, 36729, 36730, 36868, 38649, 40341, 51100, 92781, 92787, 107996, 108001, 120834
Bos	http://fossilworks.org	11803, 21197, 22584, 32093, 32113, 32124, 34105, 36134, 36136, 40497, 40692, 40695, 42866, 43008 43016, 43619, 43645, 43657, 43657, 43664, 43689, 43699, 43701, 43702, 44090, 48890, 49087, 49089, 49092, 51817, 60530, 67660, 73757, 73758, 73760, 73761, 92786, 96782, 107875, 109703, 115167, 184245
Canis	http://fossilworks.org	11803, 20123, 20126, 20127, 20129, 20130, 20134, 20137, 20138, 20143, 20143, 20148, 20150, 20150, 20150, 20157, 20166, 20173, 20178, 20187, 20205, 20237, 20273, 20273, 20277, 20280, 20281, 20283, 20283, 20283, 20285, 20285, 20289, 20290, 20290, 20293, 20295, 20295, 20297, 20299, 20301, 20302, 20302, 20302, 20302, 20302, 20308, 20319, 20323, 20327, 20327, 20329, 20329, 20334, 20335, 20342, 20342, 20342, 20346, 20347, 20347, 20351, 20351, 20360, 20375, 20376, 20387, 20387, 20398, 20400,

bioRxiv preprint doi: https://doi.org/10.1101/505131; this version posted December 23, 2018. The copyright holder for this preprint (which was not certified by peer review) is the author/funder. All rights reserved. No reuse allowed without permission.

20400, 20401, 20415, 20417, 20419, 20434, 20454, 20477, 20479, 20479, 20491, 20491, 20494, 20495, 20498, 20498, 20499, 20500, 20500, 20501, 20501, 20503, 20504, 20506, 20514, 20520, 20528, 20530, 20530, 20532, 20536, 20537, 20556, 20556, 20558, 20559, 20567, 20569, 20569, 20572, 20573, 20580, 20590, 20593, 20594, 20600, 20600, 20600, 20612, 20615, 20617, 20619, 20619, 20624, 20626, 20628, 20629, 20635, 20636, 20638, 20639, 20641, 20641, 20642, 20642, 20644, 20646, 20653, 21276, 21276, 21276, 21277, 21277, 21294, 21296, 21709, 21822, 21961, 34010, 34105, 34269, 34269, 34269, 34330, 34382, 34925, 34926, 34927, 34985, 35045, 35467, 35472, 36134, 36206, 36214, 36219, 36220, 40497, 40695, 40808, 42866, 42866, 43008, 43008, 43016, 43617, 43618, 43619, 43629, 43630, 43631, 43632, 43645, 43649, 43649, 43650, 43651, 43653, 43653, 43654, 43657, 43664, 43664, 43666, 43689, 43699, 43702, 44090, 48587, 48889, 48890, 48893, 48908, 48910, 48911, 49089, 49093, 49093, 49094, 49814, 49816, 49999, 50196, 50198, 50199, 50249, 50258, 50258, 50259, 51100, 63150, 63335, 63427, 63515, 70704, 71277, 71286, 71303, 71303, 71308, 71316, 71338, 71342, 71345, 71346, 71346, 73752, 73752, 73761, 73845, 74141, 74292, 74292, 74292, 74953, 75995, 76059, 76059, 79548, 79581, 79582, 79621, 79632, 79683, 79683, 79757, 79918, 79919, 82258, 82530, 84181, 85159, 85314, 90036, 90070, 92787, 93103, 93103, 93141, 93141, 93181, 93181, 93181, 93182, 93182, 93251, 93251, 93251, 93259, 93277, 93281, 93281, 93281, 93329, 93332, 93332, 93332, 93332, 93333, 93333, 93379, 93379, 93527, 93528, 93828, 94331, 96974, 101897, 101898, 101899, 103991, 104664, 104664, 104758, 104797, 115167, 115167, 115184, 115188, 144976, 145366, 145500, 145500, 150336, 150336, 150336, 150336, 150336, 154722, 154722, 154771, 154771, 154804, 154805, 154805, 154805, 154910, 154921, 155393, 155393, 155393, 155409, 155409, 159674, 159675, 159676,

bioRxiv preprint doi: https://doi.org/10.1101/505131; this version posted December 23, 2018. The copyright holder for this preprint (which was not certified by peer review) is the author/funder. All rights reserved. No reuse allowed without permission.

		159677, 159678, 159679, 159680, 184245
Capra	http://fossil works.org	11803, 22584, 32059, 32062, 32082, 32086, 34985, 43008, 43008, 43645, 43657, 43657, 43689, 43689, 43701, 48890, 90036, 184245
Equus	http://fossil works.org	22626, 22627, 26548, 26550, 27671, 27679, 28221, 28222, 28225, 28621, 32090, 32090, 32090, 32093, 32093, 32113, 32113, 32113, 32115, 32115, 32115, 32119, 32124, 32124, 32125, 32126, 32126, 32126, 32138, 32138, 34010, 34105, 34269, 34330, 34382, 34382, 34842, 34848, 34925, 34926, 34927, 34981, 34985, 34985, 35045, 35180, 35928, 35930, 36015, 36134, 36136, 36206, 36214, 36214, 36219, 36219, 36220, 36220, 36706, 37999, 38314, 40258, 40259, 40259, 40259, 40262, 40496, 40497, 40695, 40695, 40808, 40808, 40808, 40984, 41740, 42866, 43008, 43008, 43013, 43015, 43016, 43018, 43617, 43618, 43619, 43619, 43628, 43629, 43629, 43630, 43630, 43631, 43631, 43632, 43645, 43649, 43650, 43657, 43664, 43664, 43664, 43701, 43702, 43702, 43704, 43704, 44090, 47832, 48581, 48587, 48592, 49087, 49087, 49087, 49089, 49092, 49813, 49813, 49814, 49814, 49816, 49816, 49816, 49989, 49989, 49999, 50049, 50049, 50056, 50059, 50196, 50198, 50199, 50247, 50257, 50257, 50258, 50259, 50260, 51187, 51188, 51817, 58089, 58421, 63337, 63424, 63515, 67660, 67660, 67660, 68070, 70704, 71265, 71267, 71270, 71277, 71278, 71279, 71283, 71284, 71286, 71287, 71290, 71294, 71296, 71303, 71306, 71307, 71308, 71314, 71322, 71331, 71332, 71334, 71345, 71346, 73686, 73691, 73693, 73720, 73721, 73722, 73726, 73752, 73757, 73757, 73759, 73760, 73761, 73763, 74141, 74142, 74144, 74235, 74292, 74293, 74294, 74336, 74336, 74361, 74470, 74471, 74498, 74954, 76059, 76059, 76060, 76060, 76060, 76068, 77754, 78577, 78580, 79548, 79548, 79581, 79582, 79634, 79654, 79750, 79759, 79768, 79778, 79919, 80233, 82530, 83069, 83072, 83073, 84195, 85144, 85156, 85159, 85314, 92786, 93103, 93103, 93103, 93103, 93141, 93142, 93143, 93178, 93181, 93182,

bioRxiv preprint doi: https://doi.org/10.1101/505131; this version posted December 23, 2018. The copyright holder for this preprint (which was not certified by peer review) is the author/funder. All rights reserved. No reuse allowed without permission.

		93244, 93246, 93251, 93251, 93259, 93266, 93275, 93277, 93281, 93281, 93332, 93332, 93379, 93379, 93483, 93486, 93527, 93555, 93555, 93828, 96974, 103358, 104032, 104038, 104045, 104046, 104661, 104662, 104662, 104696, 104697, 104698, 107875, 109703, 109704, 113257, 115167, 140934, 140934, 142158, 142160, 142327, 144517, 144976, 145500, 148417, 154722, 154771, 154771, 154773, 154804, 154805, 154910, 154921, 154936, 155393, 155393, 155409, 159681, 162126, 162127, 183460, 185519
Homo	http://fossilworks.org	14243, 21277, 21294, 21337, 21360, 21368, 21402, 21402, 21403, 21403, 21413, 21413, 21415, 21441, 21441, 21449, 21455, 21455, 21514, 21520, 21822, 21970, 22466, 22499, 22584, 22618, 22622, 22622, 32059, 34269, 36016, 36134, 42866, 43631, 43704, 50199, 51100, 51188, 67660, 68020, 68055, 68056, 68058, 68063, 68064, 68066, 68067, 68068, 68070, 68474, 74292, 83069, 83072, 90070, 92781, 92786, 92787, 93141, 93521, 93523, 93524, 93537, 93597, 107997, 107999, 115167, 115188, 120834, 125671, 125672, 154805, 155393, 182079, 182940, 184245
Macaca	http://fossilworks.org	13293, 13293, 13293, 13293, 36206, 36729, 36730, 36868, 38649, 40341, 40341, 40341, 43655, 43695, 43700, 48891, 48912, 49816, 50196, 50259, 51100, 92781, 92781, 92787, 92787, 93521, 93523, 93524, 101899, 107997, 120834, 176213
Odocoileus	http://fossilworks.org	13066, 20124, 20125, 20126, 20127, 20128, 20129, 20138, 20142, 20143, 20155, 20169, 20178, 20187, 20199, 20258, 20272, 20281, 20289, 20290, 20295, 20299, 20302, 20307, 20308, 20318, 20319, 20323, 20327, 20342, 20347, 20351, 20354, 20382, 20384, 20385, 20387, 20390, 20400, 20401, 20403, 20415, 20417, 20431, 20440, 20442, 20454, 20475, 20477, 20478, 20479, 20482, 20491, 20492, 20494, 20495, 20520, 20530, 20555, 20556, 20558, 20569, 20571, 20572, 20573, 20579, 20580, 20581, 20585, 20586, 20587, 20593, 20594, 20595, 20600, 20602, 20603, 20604, 20608, 20609, 20612, 20613, 20615, 20622, 20624, 20629, 20633, 20634, 20635, 20636, 20638,

bioRxiv preprint doi: https://doi.org/10.1101/505131; this version posted December 23, 2018. The copyright holder for this preprint (which was not certified by peer review) is the author/funder. All rights reserved. No reuse allowed without permission.

		20639, 20640, 20642, 20644, 20647, 20650, 20653, 34269, 34269, 58089, 63227, 63401, 63515, 71267, 71278, 71294, 71345, 71346, 73752, 74142, 74235, 74292, 74361, 74470, 74496, 74953, 74954, 76060, 79581, 79582, 79630, 79655, 79667, 79919, 82258, 83072, 84195, 85156, 85314, 93103, 93143, 93182, 93208, 93250, 93259, 93266, 93281, 93281, 93332, 93379, 93527, 93528, 103358, 103991, 104662, 104697, 104758, 107875, 124089, 124198, 124199, 133630, 144976, 145500, 145505, 154722, 154771, 154773, 154804, 154805, 154910, 154921, 155393, 155409, 183460, 185519, 190114, 190115, 190116
Ovis	http://fossilworks.org	20272, 20273, 20297, 20428, 20472, 20477, 20615, 20621, 35045, 36729, 36730, 74176, 74953, 74954, 79548, 85144, 93141, 93181, 93277, 93278, 93281, 93339, 93528, 93555, 115167, 155393
Ponginae	http://fossilworks.org	13293, 38649, 40341, 51100, 92781, 92781, 92781, 92781, 93524, 107995, 107996, 107997, 107999, 108000, 108001, 108001, 108001, 120834
Rhinopithecus	http://fossilworks.org	13293, 36724, 40341, 92787, 120834
Sus	http://fossilworks.org	11803, 13293, 21893, 34679, 34981, 34985, 36134, 36206, 36214, 36729, 36730, 36868, 38649, 38649, 40341, 40808, 40984, 43008, 43016, 43618, 43629, 43645, 43653, 43655, 43657, 43657, 43664, 43664, 43689, 43697, 43699, 43700, 43701, 44090, 44092, 47832, 48891, 49087, 49089, 49092, 49813, 49814, 49815, 49816, 50196, 50199, 50258, 50259, 51100, 51100, 58421, 90036, 92781, 92781, 92781, 92787, 92787, 93521, 93523, 93523, 93524, 93828, 109704, 120834, 120834, 184245,
Ursus	http://fossilworks.org	11803, 13293, 20273, 20290, 20297, 20302, 20302, 20302, 20302, 20354, 20479, 20491, 20520, 20554, 20556, 20569, 20571, 20572, 20600, 20636, 20647, 34010, 34012, 34269, 34330, 34368, 34842, 34848, 34925, 35045, 35045, 35472, 35476, 36206, 36214, 36214, 36219, 36220, 36729, 36730, 36868, 38649, 40341, 40497, 40808, 43008, 43008, 43016, 43617, 43617, 43618, 43619, 43628, 43629, 43630, 43643,

bioRxiv preprint doi: https://doi.org/10.1101/505131; this version posted December 23, 2018. The copyright holder for this preprint (which was not certified by peer review) is the author/funder. All rights reserved. No reuse allowed without permission.

		43645, 43653, 43654, 43655, 43664, 43666, 43666, 43689, 43697, 43699, 43701, 43702, 44092, 47832, 48587, 48890, 48911, 48912, 49087, 49089, 49093, 49813, 49816, 49816, 49999, 50196, 50196, 50198, 50199, 50199, 50257, 50258, 50259, 50259, 50990, 51100, 58419, 63229, 71345, 73686, 73691, 73726, 73752, 74139, 74140, 74141, 74235, 74235, 74292, 74292, 74496, 74954, 76059, 76060, 77754, 79548, 81672, 81673, 81674, 81675, 81676, 81677, 81678, 81679, 82258, 82530, 84181, 84195, 90036, 92781, 92781, 92787, 92787, 93103, 93141, 93182, 93250, 93277, 93278, 93278, 93279, 93332, 93486, 93524, 93527, 93828, 93837, 96782, 101897, 101898, 101899, 103991, 104662, 104664, 104669, 104681, 107956, 109704, 120834, 154722, 154773, 154936, 155393, 155409, 162543, 162544, 184245
Software and Algorithm		
Soapnuke (v1.5.6)	[52]	https://libraries.io/github/BGI-flexlab/SOAPnuke
BWA (v0.7.17)	[53]	http://bio-bwa.sourceforge.net
PSMC	[4]	https://github.com/lh3/psmc
QGIS(v3.2.3)		https://qgis.org/en/site/
N_e curve analysis	This paper	https://github.com/Solenyalyl/Ne-curve-analysis

CONTACT FOR REAGENT AND RESOURCE SHARING

Further information and requests for resources and reagents should be directed to and will be fulfilled by the Lead Contact, Shuaicheng Li (shuaicli@gmail.com).

METHOD DETAILS

Mammal and fossil distribution

bioRxiv preprint doi: https://doi.org/10.1101/505131; this version posted December 23, 2018. The copyright holder for this preprint (which was not certified by peer review) is the author/funder. All rights reserved. No reuse allowed without permission.

Mammalian SRA data came from different studies, and not all of their locations were recorded. Mammalian place of origin was regarded as the location if a sample was collected from the zoo; domestication location was taken to be the location if it was assured; and when it was ambiguous, sampling location was regarded as the location. For each of the remaining samples without location recorded, we researched the species distribution in the world and then chose a representative place as the location. Our mammals were distributed among 15 genera, and their fossil records were found in http://fossilworks.org/ except for *Pan* and *Gorilla*. Those fossils originated in the Calabrian (1.8-0.781 mya), middle Pleistocene (0.781-0.126 mya) or late Pleistocene (0.126-0.0117 mya). Mammal location and fossil data distribution were plotted using QGIS (Figure S1 and Figure S3).

Data collection and preprocessing

We downloaded mammalian Illumina sequence data from public SRA datasets (https://www.ncbi.nlm.nih.gov/sra/), Chinese BAM files were downloaded from https://www.ebi.ac.uk/, and non-Chinese BAM files were collected from http://www.internationalgenome.org/. Including 60 specimens from 35 species, these SRA data were sequenced by Illumina paired-end sequencing technology using different sequencing platforms, therefore our first step was transforming all the Illumina sequence data into uniform Q+33 Illumina format. All the raw sequencing reads were filtered by

bioRxiv preprint doi: https://doi.org/10.1101/505131; this version posted December 23, 2018. The copyright holder for this preprint (which was not certified by peer review) is the author/funder. All rights reserved. No reuse allowed without permission.

460 Soapnuke [52] (http://soap.genomics.org.cn/) and each was aligned to its respective
461 reference genome or the most related genome from the same genus by BWA 0.7.17 [53].
462 Samples with genome coverage depth less than 6X were excluded.
463
464 ***N_e curve generation***
465 The historical N_e curve of mammals was inferred by PSMC based on genome data [4]. A
466 PSMC-based consensus genome sequence was obtained by using 'mpileup' in
467 SAMTOOLS. When the RMS (root-mean-squared) quality of reads was below 20, their
468 covered sites were marked N for missing data. The sites whose read depths were less
469 than a third or more than twice the average depth across the genome were masked to
470 avoid collapsed regions in the assembly. When we ran PSMC, the upper limit of TRMCA
471 was set to 15, the initial θ/ρ value was set to 5 and time interval was set to
472 '1*4+25*2+1*4+1*6' as Li and Durbin [4] did. The mutation rate and generation time we
473 applied are in Table S3. The genome coverage depth, coverage ratio, and false-negative
474 ratio are in Table S2. For statistical analysis of these N_e curves see sections below.
475
476 **QUANTIFICATION AND STATISTICAL ANALYSIS**
477
478 ***PC analysis and hierarchical clustering***

bioRxiv preprint doi: https://doi.org/10.1101/505131; this version posted December 23, 2018. The copyright holder for this preprint (which was not certified by peer review) is the author/funder. All rights reserved. No reuse allowed without permission.

PCA was used to identify the principal components of N_e curves. Every N_e curve contains 58 points. We standardized these data to unit standard deviation and centralized these points approximately 0, then extracted their principal components to conduct hierarchical clustering. The distance matrix between samples was calculated from Euclidean distance and distance between two clusters was calculated by the UPGMA (unweighted pair group method with arithmetic mean) method.

N_e curve extrema analysis

To obtain the extrema of every curve, we marked increasing trends as '1' and decreasing trends as '-1' in curves, then the latter trend number was used to subtract the former trend number to obtain the extrema. '-2' and '2' represent crest and trough, respectively. To verify whether these extrema are distributed randomly, we compared these extrema with a uniform distribution to obtain Hopkins statistics. After obtaining a clustering trend, these extrema were clustered by the K-means method to get a pattern. Then we used this pattern to predict every curve extrema into seven clusters by removing those neglectable extrema (difference within 0.1).

DATA AND SOFTWARE AVAILABILITY

N_e curve analysis code is available from https://github.com/Solenyalyl/Ne-curve-analysis.

Excel table Legends

bioRxiv preprint doi: https://doi.org/10.1101/505131; this version posted December 23, 2018. The copyright holder for this preprint (which was not certified by peer review) is the author/funder. All rights reserved. No reuse allowed without permission.

499 **Table S1. N_e curve extrema seven clusters (related to Figure 2,3)**

500 **Table S2. coverage depth, coverage ratio, and false-negative ratio of 60 mammal**

501 **genomes(related to Figure 1-4)**

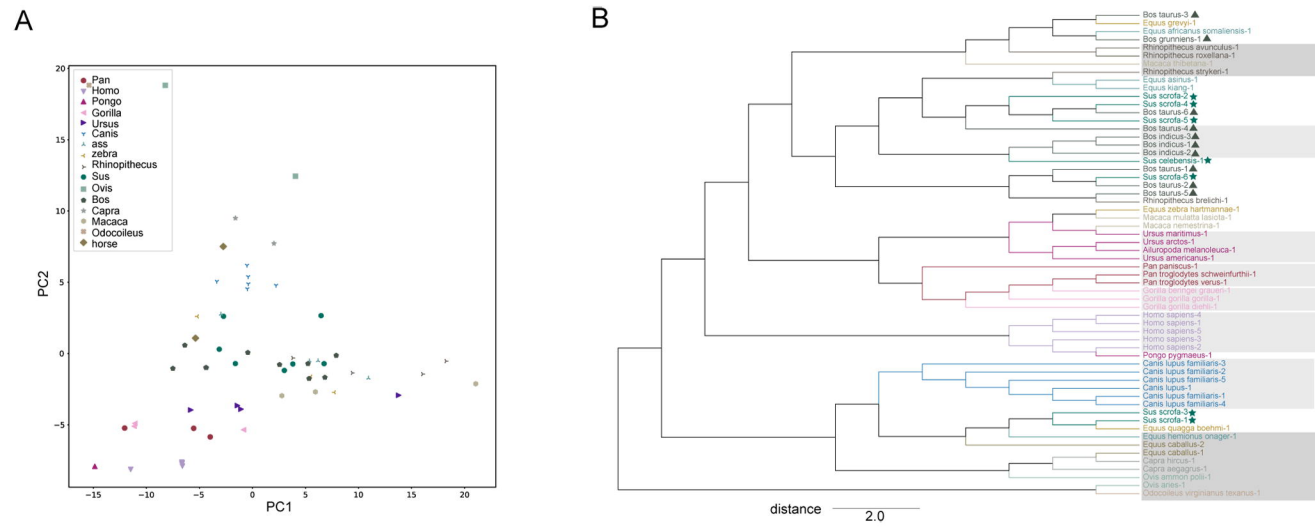
A
Pan
Homo
Pongo
Gorilla
Ursus
Canis
ass
zebra
Rhinopithecus
Sus
Ovis
Bos
Capra
Macaca
Odocoileus
horse
PC1
PC2
B
Bos taurus-3
Equus grevyi-1
Equus africanus somaliensis-1
Bos grunniens-1
Rhinopithecus avunculus-1
Rhinopithecus roxellana-1
Rhinopithecus bieti-1
Rhinopithecus strykeri-1
Equus asinus-1
Equus kiang-1
Sus scrofa-2
Sus scrofa-4
Bos taurus-6
Sus scrofa-5
Bos taurus-4
Bos indicus-3
Bos indicus-1
Bos indicus-2
Sus celebensis-1
Bos taurus-1
Sus scrofa-6
Bos taurus-2
Bos taurus-5
Rhinopithecus brelichi-1
Equus zebra hartmannae-1
Macaca mulatta lasiota-1
Macaca nemestrina-1
Ursus maritimus-1
Ursus arctos-1
Ailuropoda melanoleuca-1
Ursus americanus-1
Pan paniscus-1
Pan troglodytes schweinfurthii-1
Pan troglodytes verus-1
Gorilla beringei graueri-1
Gorilla gorilla gorilla-1
Gorilla gorilla diehli-1
Homo sapiens-4
Homo sapiens-1
Homo sapiens-5
Homo sapiens-3
Homo sapiens-2
Pongo pygmaeus-1
Canis lupus familiaris-3
Canis lupus familiaris-2
Canis lupus familiaris-5
Canis lupus-1
Canis lupus familiaris-1
Canis lupus familiaris-4
Sus scrofa-3
Sus scrofa-1
Equus quagga boehmi-1
Equus hemionus onager-1
Equus caballus-2
Equus caballus-1
Capra hircus-1
Capra aegagrus-1
Ovis ammon polii-1
Ovis aries-1
Odocoileus virginianus texanus-1
distance
2.0

Mammals

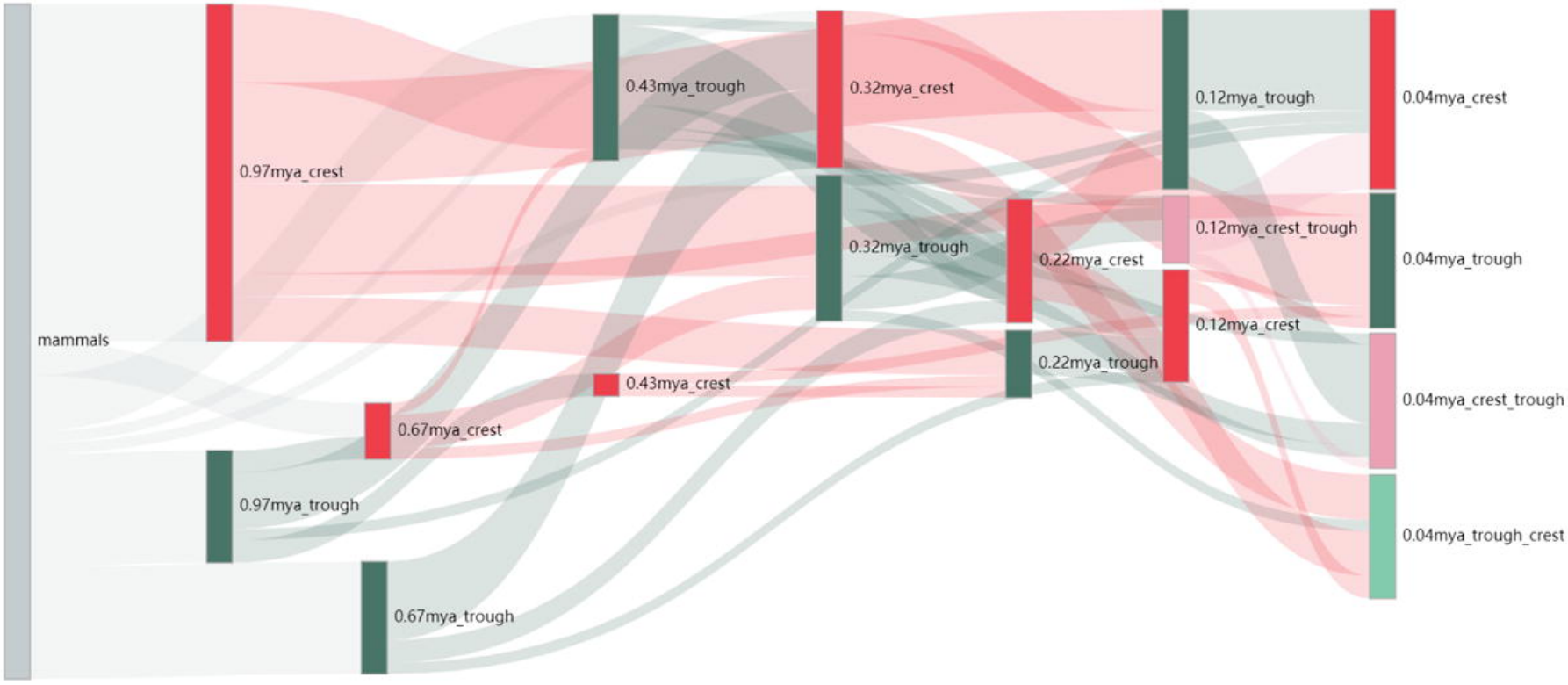
mammals
0.97mya_crest
0.97mya_trough
0.67mya_crest
0.67mya_trough
0.43mya_trough
0.43mya_crest
0.32mya_crest
0.32mya_trough
0.22mya_crest
0.22mya_trough
0.12mya_trough
0.12mya_crest_trough
0.12mya_crest
0.04mya_crest
0.04mya_trough
0.04mya_crest_trough
0.04mya_trough_crest

A

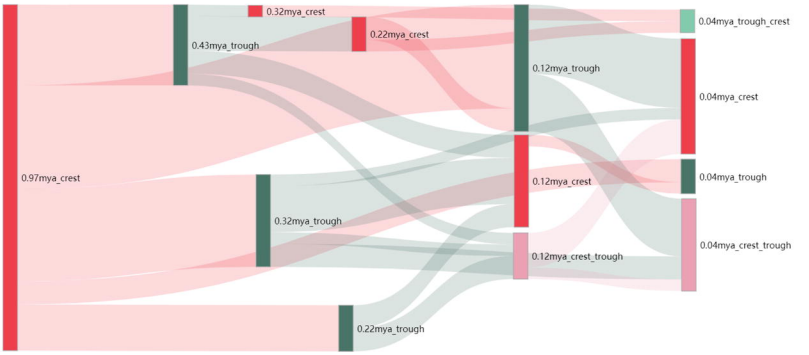
0.97mya_crest
0.43mya_trough
0.32mya_crest
0.22mya_crest
0.32mya_trough
0.22mya_trough
0.12mya_trough
0.12mya_crest
0.12mya_crest_trough
0.04mya_trough_crest
0.04mya_crest
0.04mya_trough
0.04mya_crest_trough

B

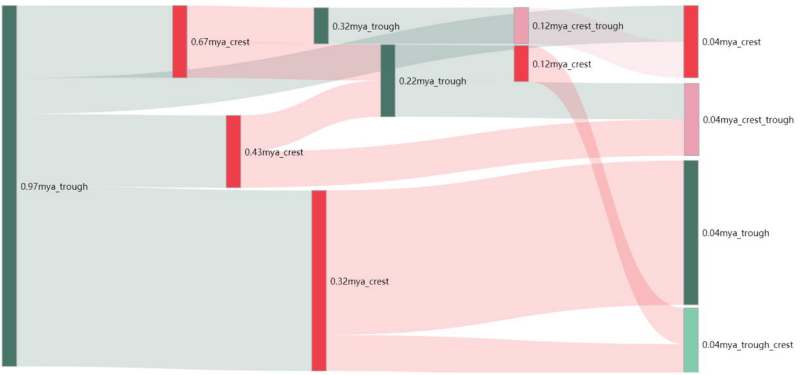
0.97mya_trough
0.67mya_crest
0.32mya_trough
0.22mya_trough
0.43mya_crest
0.32mya_crest
0.12mya_crest_trough
0.12mya_crest
0.04mya_crest
0.04mya_crest_trough
0.04mya_trough
0.04mya_trough_crest

C

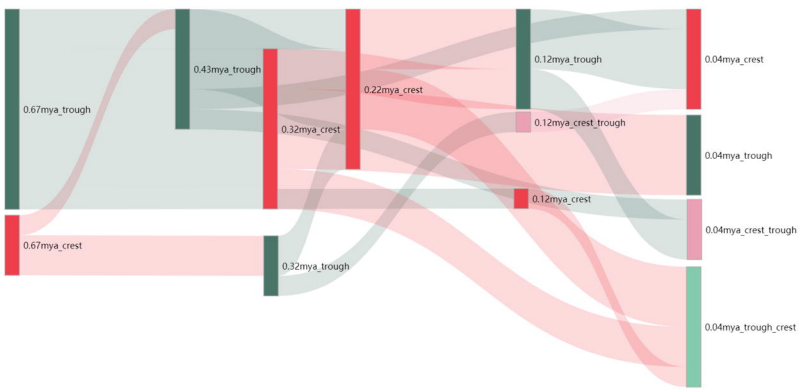
0.67mya_trough
0.67mya_crest
0.43mya_trough
0.32mya_crest
0.22mya_crest
0.32mya_trough
0.12mya_trough
0.12mya_crest_trough
0.12mya_crest
0.04mya_crest
0.04mya_trough
0.04mya_crest_trough
0.04mya_trough_crest

A

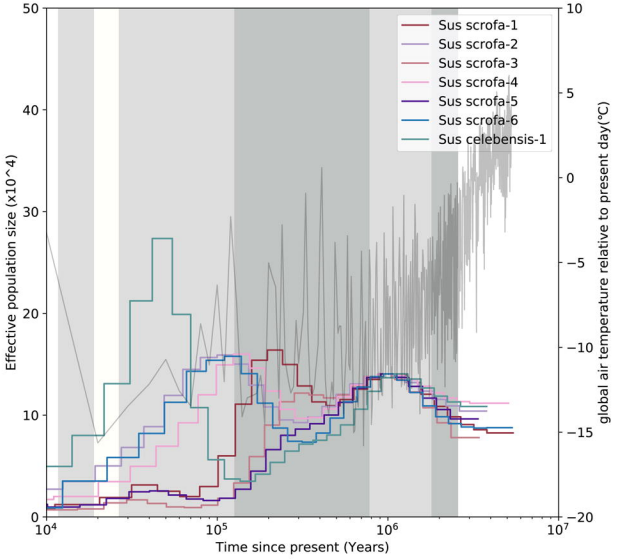
Sus scrofa-1
Sus scrofa-2
Sus scrofa-3
Sus scrofa-4
Sus scrofa-5
Sus scrofa-6
Sus celebensis-1
Effective population size (x10^4)
global air temperature relative to present day(℃)
Time since present (Years)

B

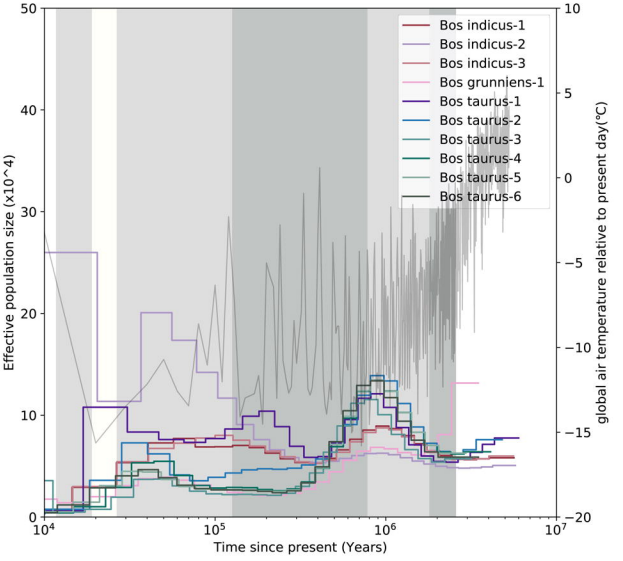
Bos indicus-1
Bos indicus-2
Bos indicus-3
Bos grunniens-1
Bos taurus-1
Bos taurus-2
Bos taurus-3
Bos taurus-4
Bos taurus-5
Bos taurus-6
Effective population size (x10^4)
global air temperature relative to present day(℃)
Time since present (Years)

C

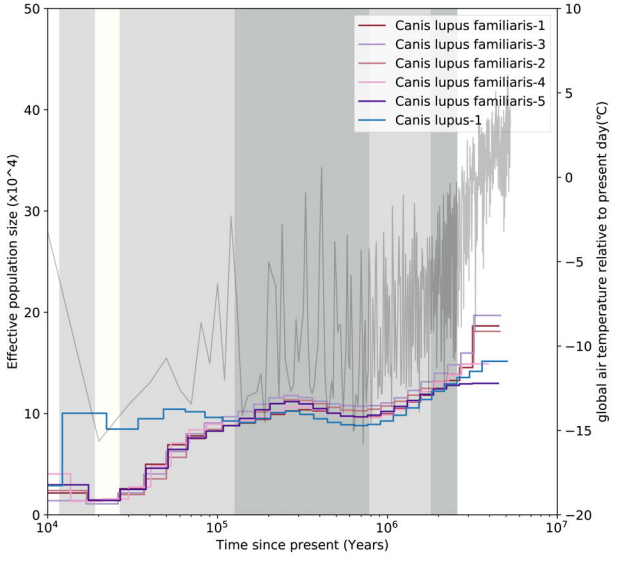
Canis lupus familiaris-1
Canis lupus familiaris-3
Canis lupus familiaris-2
Canis lupus familiaris-4
Canis lupus familiaris-5
Canis lupus-1
Effective population size (x10^4)
global air temperature relative to present day(℃)
Time since present (Years)